Highly stable kinematic nonlinear simulations using a Taylor basis

S Andersen and P N Poulsen

Department of Civil and Mechanical Engineering, Technical University of Denmark, Kgs Lyngby, Denmark

E-mail: seba@dtu.dk

Abstract. The simulation of kinematic nonlinear systems is typically very time-consuming. The computational cost is primarily related to a time-consuming evaluation of the internal restoring forces performed before each integration step. Using basis projection is a way to reduce the computational cost and, thereby, the simulation time. The present work considers a novel Taylor basis that can significantly improve the stability of the central difference time integration scheme for kinematic nonlinear simulations. It is illustrated that the time step stability limit for a kinematic nonlinear simulation using Taylor basis projection is more or less identical to the analytical stability limit derived for linear systems. Furthermore, an example shows that the time step stability limit in simulations using Taylor basis projection can be two orders of magnitude higher than the stability limit of a standard kinematic nonlinear simulation. Thus, Taylor basis projection has the potential to significantly reduce the number of time steps and, thereby, the computational cost.

1. Introduction

Numerical simulations of kinematic nonlinear dynamic structures modeled using the finite element method (FEM) are typically very time-consuming. The high computational cost is primarily related to a time-consuming element-by-element evaluation of the nonlinear internal restoring forces, followed by assembling the global equations of motion (EOMs) before executing a time step.

The computational cost associated with the assembling increases as the numerical model's size (i.e., the number of degrees of freedom) increases. Also, increasing the numerical model size (e.g., to improve the solution accuracy) introduces higher response frequencies into the model. As a consequence of this, the integration time steps need to be significantly decreased in order to maintain response stability and accuracy. The decrease in time step magnitude will increase the number of required time steps and, thereby, increase the number of internal restoring force evaluations and the computational cost.

The computational time can be efficiently decreased by reducing the number of degrees of freedom and removing some of the model's high-frequency content, potentially allowing increased time step magnitudes to be used without causing instability. A common way to do this is by projecting the discretized nonlinear EOMs onto a basis representing a reduced solution subspace. The first use of basis projection for kinematic nonlinear systems can be dated back to the work in [1, 2], where the EOMs were projected onto bases consisting of so-called mode shapes. Since then, many basis vectors have been suggested to improve the robustness and accuracy of

the simulations of kinematic nonlinear structures, cf. [3]. Among the most commonly applied basis vectors in kinematic nonlinear context are linear normal modes (also referred to as *mode shapes*), modal derivatives (MDs) [4], Ritz vectors [5], and vectors based on the proper orthogonal decomposition (POD) method [6–8]. The present work focus on MDs.

MDs were initially introduced in [4,9], where a set of equations governing the first-order MDs were derived by differentiating the linearized eigenvalue problem. However, the equations only represent an approximation to the actual governing equations. Also, they include a singular matrix from which the MDs cannot be determined directly. In order to solve the singularity issue, it has i.a. been suggested to either neglect the system's inertia or to constrain a component of the MDs, cf. [4, 10–15]. It has also been suggested to evaluate the MDs numerically using finite difference approximations, see e.g., [14–16]. In [17], a perturbation method was used to derive a set of equations governing the MDs. However, all of the mentioned approaches include some approximation.

In [18,19], a novel set of equations governing the MDs were derived from perturbation methods by introducing a Taylor series into the free undamped kinematic nonlinear EOMs. By way of an example, it was demonstrated that the MDs were consistent with the Taylor series. It was furthermore illustrated that simulations using a Taylor basis including the novel MDs display high accuracy and stability properties. The stability of the simulations using Taylor basis projection was more or less identical to the simulations of a linear system. The favorable stability feature made it possible to increase the time step magnitudes and thereby reduce the computational time of a highly nonlinear system by one order of magnitude using a Taylor basis compared to a 'standard' basis formulation, including identical basis vectors.

In [18, 19] the properties of the Taylor basis were considered for undamped structures. The present work extends the stability and accuracy analysis of the Taylor basis formulation to lightly damped structures. This is done by simulating the kinematic nonlinear response of a beam bridge exposed to moving loads with a varying load magnitude range and comparing the Taylor basis solutions with the solutions found by simulating the un-projected EOMs.

The structure of the paper is as follows. Section 2 presents the discretized EOMs representing a kinematic nonlinear system. In section 3 a description of Taylor basis projection is given. Next, in Section 4, the properties of the simulations using a Taylor basis are illustrated by way of an example. Finally, in Section 5, a conclusion is given.

2. The governing kinematic nonlinear equations of motion

The discretized governing Equations of Motion (EOMs) for a kinematic nonlinear system containing n degrees of freedom (DOFs) can be written as

$$\mathbf{M}\ddot{\mathbf{V}}(t) + \mathbf{C}\dot{\mathbf{V}}(t) + \mathbf{g}(\mathbf{V}(t)) = \mathbf{F}(t) \tag{1}$$

$\mathbf{V}(t)$ is an $n \times 1$ vector containing the global displacements dependent on time t, $\mathbf{M}$ is an $n \times n$ mass matrix, $\mathbf{C}$ is an $n \times n$ viscous damping matrix, $\mathbf{F}(t)$ is an $n \times 1$ time dependent vector representing the external load and $\mathbf{g}(\mathbf{V}(t))$ is an $n \times 1$ vector representing the internal restoring forces. The notation $\dot{()} = d()/dt$ defines a time derivative.

3. Taylor Basis Projection

Basis projection can reduce the number of DOFs in the EOMs to be solved in every integration step and simultaneously remove some of the non-physical high-frequency content. In [19] the truncated Taylor series in (2) is suggested as basis for kinematic nonlinear simulations.

$$\mathbf{V}(\mathbf{s}) = \sum_{i=1}^{N} \boldsymbol{\varphi}_i s_i + \sum_{i=1}^{N} \sum_{j=1}^{i} \partial\boldsymbol{\varphi}_{ij} s_i s_j \tag{2}$$

The first term on the right-hand side of the Taylor series in (2) includes N mode shapes, $\boldsymbol{\varphi}_i$, multiplied by N time-dependent reduced modal subspace co-ordinates $s_i(t)$, $i \in [1,N]$. The second term on the right hand side includes $H = \frac{1}{2}(N + N^2)$ first-order modal derivatives (MDs), $\partial\boldsymbol{\varphi}_{ij}$, defined as

$$\partial\boldsymbol{\varphi}_{ij} = \frac{\partial\boldsymbol{\varphi}_i}{\partial s_j} + (1 - \delta_{ij})\frac{\partial\boldsymbol{\varphi}_j}{\partial s_i} \tag{3}$$

where δ_{ij} is the Kronecker delta. The MDs are multiplied by a second-order modal subspace coordinate product consisting of the same modal coordinates multiplied onto the mode shapes in the first term. Thus, the Taylor series includes a total of $N + H$ basis vectors but only N unknown modal coordinates to be determined in every time integration step. The Taylor series in (2) can be formulated as a compact matrix product

$$\mathbf{V}(\mathbf{s}) = \boldsymbol{\Phi}_{\mathrm{T}}\mathbf{s}_{\mathrm{T}} \tag{4}$$

where $\boldsymbol{\Phi}_T$ is referred to as the *Taylor basis matrix* and $\mathbf{s}_{\mathrm{T}}$ as the *Taylor co-ordinate vector*. These are given as

$$\boldsymbol{\Phi}_{\mathrm{T}} = \begin{bmatrix}\boldsymbol{\varphi}_1, & \boldsymbol{\varphi}_2, & \ldots & \boldsymbol{\varphi}_N, & \partial\boldsymbol{\varphi}_{11}, & \partial\boldsymbol{\varphi}_{21}, & \ldots & \partial\boldsymbol{\varphi}_{NN}\end{bmatrix} \tag{5}$$

$$\mathbf{s}_{\mathrm{T}} = \begin{bmatrix}s_1, & s_2, & \ldots & s_N, & s_1s_1, & s_2s_1, & \ldots & s_Ns_N\end{bmatrix}^T \tag{6}$$

Inserting the Taylor series into the governing EOMs in the case of zero damping and zero loading, it was shown from perturbation methods in [18] that the linearized eigenvalue problem in (7) governs the mode shapes.

$$\left(\mathbf{K}_{\mathrm{T}}(\mathbf{V}) - \omega_i^2\mathbf{M}\right)\boldsymbol{\varphi}_i = \mathbf{0} \tag{7}$$

The matrix $\mathbf{K}_{\mathrm{T}}(\mathbf{V})$ in (7) represents the displacement-dependent tangent stiffness matrix, and ω_i is the natural angular frequency associated with the i'th mode shape. The perturbation method furthermore showed that the equations governing the first-order MDs in the zero displacement state are given as

$$\left[\mathbf{K}_{\mathrm{T}}(\mathbf{0}) - (\omega_j + \omega_i)^2\mathbf{M}\right]\frac{1}{2}\left(\frac{\partial\boldsymbol{\varphi}_i}{\partial s_j} + \frac{\partial\boldsymbol{\varphi}_j}{\partial s_i}\right) = \left[\alpha\mathbf{M} - \frac{\partial\mathbf{K}_{\mathrm{S}}(\mathbf{0})}{\partial s_i}\right]\boldsymbol{\varphi}_j \tag{8}$$

with $\mathbf{K}_{\mathrm{T}}(\mathbf{0})$ and $\mathbf{K}_{\mathrm{S}}(\mathbf{0})$ defining, respectively, the tangent and secant stiffness matrices at zero displacements. The parameter α is a scalar defined as

$$\alpha = \frac{\boldsymbol{\varphi}_j^T}{\boldsymbol{\varphi}_j^T\mathbf{M}\boldsymbol{\varphi}_j}\left(\frac{\partial\mathbf{K}_{\mathrm{S}}(\mathbf{0})}{\partial s_i}\boldsymbol{\varphi}_j - \frac{\partial\mathbf{K}_{\mathrm{S}}(\mathbf{0})}{\partial s_j}\boldsymbol{\varphi}_i\right) \tag{9}$$

Projecting the EOMs in (1) onto the Taylor basis leads to a system of second-order differential equations with displacement and velocity-dependent coefficients in the reduced subspace. The projected equations are formulated as

$$\bar{\mathbf{m}}(\mathbf{s})\ddot{\mathbf{s}} + \bar{\mathbf{c}}(\mathbf{s},\dot{\mathbf{s}})\dot{\mathbf{s}} + \bar{\mathbf{g}}(\mathbf{s}) = \bar{\mathbf{f}}(\mathbf{s},t) \tag{10}$$

with the following matrix and vector definitions

$$\bar{\mathbf{m}}(\mathbf{s}) = \mathbf{U}(\mathbf{s})^T\boldsymbol{\Phi}_{\mathrm{T}}^T\mathbf{M}\boldsymbol{\Phi}_{\mathrm{T}}\mathbf{U}(\mathbf{s}) \tag{11}$$

$$\bar{\mathbf{c}}(\mathbf{s},\dot{\mathbf{s}}) = \mathbf{U}(\mathbf{s})^T\boldsymbol{\Phi}_{\mathrm{T}}^T\left(2\mathbf{M}\boldsymbol{\Phi}_{\mathrm{T}}\mathbf{P}(\dot{\mathbf{s}}) + \mathbf{C}\boldsymbol{\Phi}_{\mathrm{T}}\mathbf{U}(\mathbf{s})\right) \tag{12}$$

$$\bar{\mathbf{g}}(\mathbf{s}) = \mathbf{U}(\mathbf{s})^T\boldsymbol{\Phi}_{\mathrm{T}}^T\mathbf{g}(\boldsymbol{\Phi}_{\mathrm{T}}\mathbf{s}_T) \tag{13}$$

$$\bar{\mathbf{f}}(\mathbf{s},t) = \mathbf{U}(\mathbf{s})^T\boldsymbol{\Phi}_{\mathrm{T}}^T\mathbf{F}(t) \tag{14}$$

The matrices $\mathbf{U}(\mathbf{s})$ and $\mathbf{P}(\dot{\mathbf{s}})$ are transformation matrices of dimension $(N + H) \times N$, cf. [19].

4. Example - Nonlinear Beam Bridge

The precision and stability properties of the suggested Taylor basis are illustrated by an example. A beam bridge is sketched in Figure 1. It consists of a horizontal steel bridge girder of total length 3ℓ and two vertical concrete bridge piers of height h. The piers and the girder are rigidly connected in their intersection points. The bridge is supported by simple supports at the bridge girder endpoints, and by rigid supports at the pier feet. The vertical downwards displacement of the bridge girder is referred to as $u_g(x,t)$.

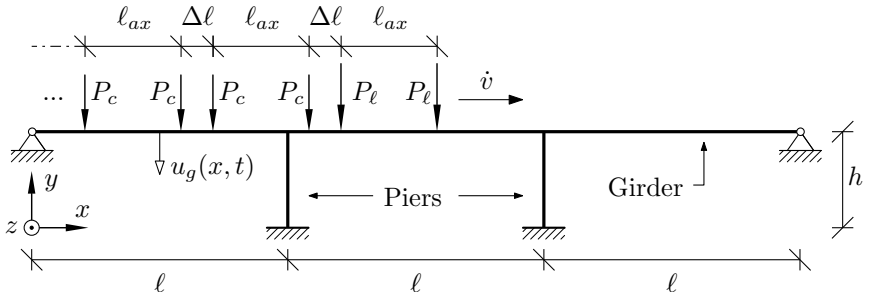

Figure 1. Beam bridge exposed to train loads.

Table 1 lists the assumed bridge parameters, including Young's moduli, E, densities per unit length, ρ, cross-sectional areas, A, damping ratios, ζ, and second moment of areas, I, with respect to rotation around the $z-$axis.

Table 1. Beam bridge parameters.

Parameter	Unit	Bridge Girder	Bridge Piers
ℓ	m	100	-
h	m	-	20
E	GPa	200	36
A	m^2	0.27	14.60
I	m^4	0.18	4.87
ρ	kg/m	3,206	36,500
ζ	-	2%	2%

The beam bridge is modeled with 2D Euler-Bernoulli beam elements. For a detailed element description, see e.g., [18]. The applied mesh consists of 24 equally long elements along the bridge girder and six equally long elements in each bridge column. The given mesh ensures that the first three natural angular frequencies have converged down to the second decimal.

The beam bridge is loaded by a train traveling at a constant velocity, $\dot{v}$. The train consists of a locomotive of weight W_ℓ and N_c carriages each of weight W_c. The train load is transferred onto the bridge through two train axles installed at each train carriage and locomotive with a length spacing ℓ_{ax}, see Figure 1. The distance between the train axles of two neighboring train carriages is $\Delta\ell$. The weight is distributed equally between the axles, i.e., the loads entering the bridge are $P_\ell = \frac{1}{2}W_\ell$ and $P_c = \frac{1}{2}W_c$. The loads are modeled as moving massless loads, and the applied load parameters are listed in Table 2.

The locomotive front axle enters the bridge at time $t = 0$ s. With the velocity given in Table 2, the last carriage axle enters the bridge at time $t_{N_c}^{\text{enter}} = 24.73$ s. Furthermore, the last train axle arrives at the end of the first bridge span ($x = \ell$) at time $t_{N_c}^{\text{exit}} = 29.95$ s.

Table 2. Load parameters.

Parameter	Unit	Magnitude
$W_\ell = 2P_\ell$	MN	1
$W_c = 2P_c$	kN	650
$\dot{v}$	km/h	69
N_c	-	20
ℓ_{ax}	m	18
$\Delta\ell$	m	6

4.1. Kinematic Nonlinear Bridge Response

The bridge girder displacement at $x = \ell/2$, $\bar{u}_g(t) = u_g(\ell/2, t)$, is considered. In Figure 2, the linear and the kinematic nonlinear displacement are plotted for a time interval $t \in$ [0,50 s].

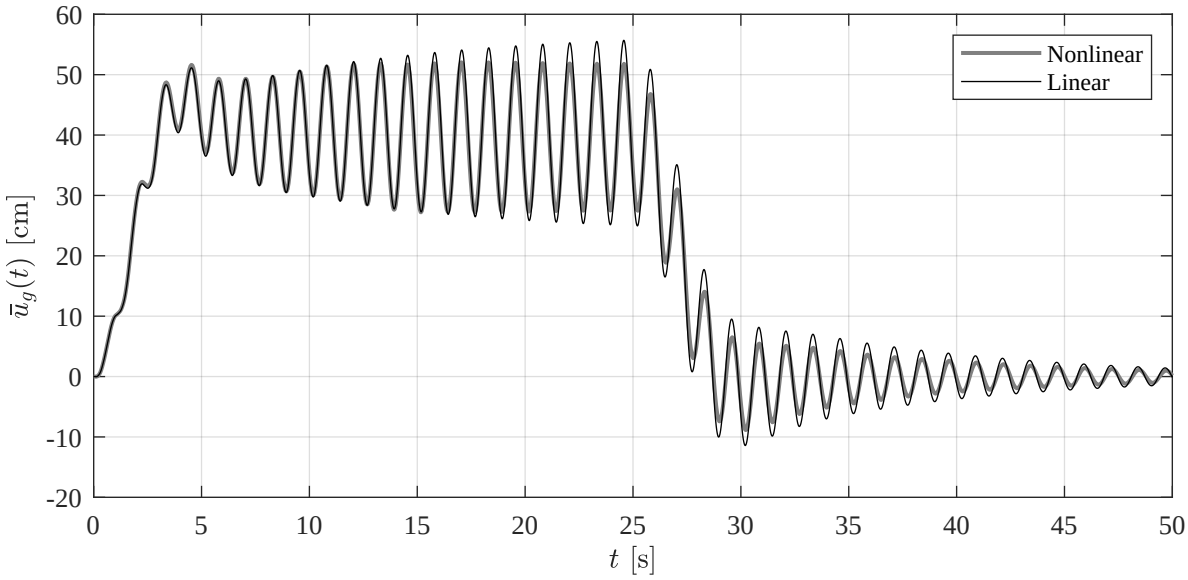

Figure 2. Linear and kinematic nonlinear displacement $\bar{u}_g(t) = u_g(\ell/2, t)$.

The nonlinear response is evaluated by solving the EOMs in (1), and the linear response is evaluated by solving the equations in (1) with $\mathbf{g}(\mathbf{V}(t))$ replaced by $\mathbf{K}_{\mathrm{S}}(\mathbf{0})\mathbf{V}(t)$. The linear and nonlinear central difference method (CDM) time integration schemes with a constant time step $\Delta t = 0.56$ ms are used.

The linear and nonlinear responses $\bar{u}_g(t)$ are initiated as the locomotive front axle enters the bridge girder at time $t = 0$ s. The responses grow significantly within the first response cycles, after which they oscillate about a deformed position of approximately 40 cm. The nonlinear displacement reaches a steady state response after approximately 15 seconds. In contrast, the linear response amplitude keeps increasing steadily until around $t \approx t_{N_c}^{\mathrm{enter}}$, where the last carriage axle load enters the bridge. After this point in time, the total load on the bridge begins to decrease as the axle loads exit the bridge. As a result, the response equilibrium points drop steadily toward zero over a few response cycles. After the last axle load has reached the first bridge span ($x = \ell$) at time $t_{N_c}^{exit}$, the displacements display a damped behavior with a decaying amplitude oscillating around the zero displacement axis.

The nonlinear response reaches a maximum response amplitude of nearly 52 cm within the considered time period, whereas the linear response amplitude reaches 56 cm. A smaller response in the nonlinear case is expected as the stiffness of kinematic nonlinear systems increases for increasing displacements. Based on these observations, the given example is concluded to be a relevant case study for illustrating the accuracy and stability of the introduced Taylor basis.

4.2. Simulation accuracy using Taylor basis projection

The response accuracy associated with Taylor basis projection is illustrated next. This is done by comparing the solution of the projected EOMs in (10) with the solution of the EOMs in (1). A Taylor basis, including the three mode shapes associated with the three lowest natural angular frequencies and their associated MDs, is used; see (15).

$$\mathbf{V}(\mathbf{s}) = \underbrace{\begin{bmatrix} \boldsymbol{\varphi}_1 & \boldsymbol{\varphi}_2 & \boldsymbol{\varphi}_3 & \partial\boldsymbol{\varphi}_{11} & \partial\boldsymbol{\varphi}_{21} & \partial\boldsymbol{\varphi}_{22} & \partial\boldsymbol{\varphi}_{31} & \partial\boldsymbol{\varphi}_{32} & \partial\boldsymbol{\varphi}_{33} \end{bmatrix}}_{\boldsymbol{\Phi}_{\mathrm{T}}} \underbrace{\begin{Bmatrix} s_1 \\ s_2 \\ s_3 \\ s_1 s_1 \\ s_2 s_1 \\ s_2 s_2 \\ s_3 s_1 \\ s_3 s_2 \\ s_3 s_3 \end{Bmatrix}}_{\mathbf{s}_{\mathrm{T}}} \tag{15}$$

The mode shapes included in (15) are characterized primarily by bending in the bridge girder, see Figure 3. Mode one is antimetric, whereas modes two and three are symmetric with respect to a vertical axis through the bridge girder center point. The modes are scaled by individual factors α specified in each subfigure.

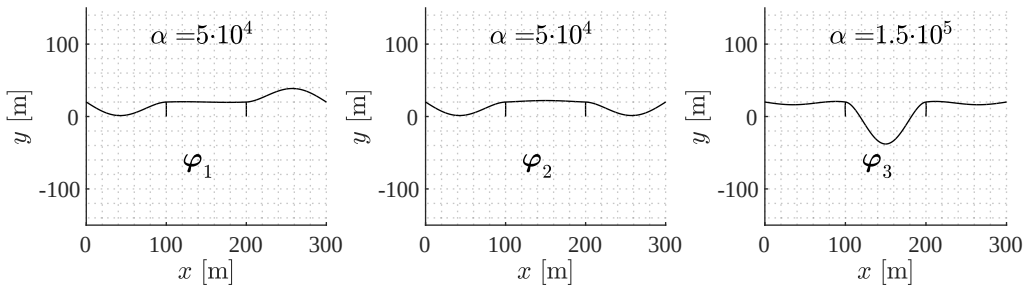

Figure 3. Mode shapes.

The natural angular frequencies associated with the mode shapes in Figure 3 are listed in Table 3. The lowest two frequencies are seen to be almost identical.

Table 3. Natural angular frequencies.

Frequency	Unit	Magnitude
ω_1	rad/s	5.01
ω_2	rad/s	5.02
ω_3	rad/s	7.16

The MDs included in (15) are evaluated by use of Equation (8) and plotted in Figure 4. In contrast to the mode shapes in Figure 3, the MDs are characterized by bending in both the bridge girder and the bridge columns. Furthermore, the scaling factors α applied in Figure 3 and Figure 4 indicate that the magnitudes of the MDs are significantly smaller than the mode shape magnitudes.

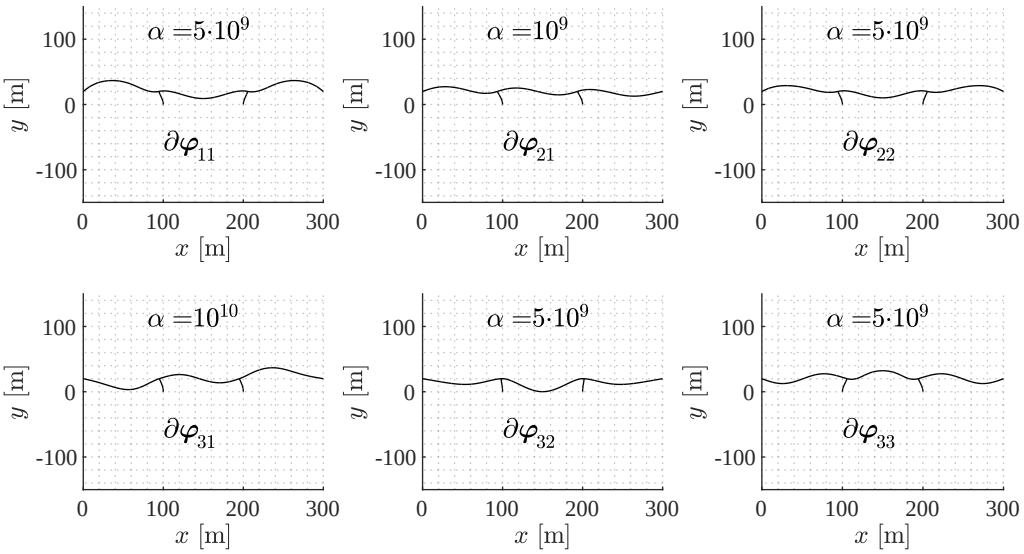

Figure 4. Modal derivatives.

Table 4 lists the natural angular frequencies ω_{ij} associated with the MDs. These are approximated by the use of Rayleigh's quotient as

$$\omega_{ij}^2 = \frac{\partial\boldsymbol{\varphi}_{ij}^T \mathbf{K}_{\mathrm{T}}(\mathbf{0}) \partial\boldsymbol{\varphi}_{ij}}{\partial\boldsymbol{\varphi}_{ij}^T \mathbf{M} \partial\boldsymbol{\varphi}_{ij}} \tag{16}$$

From Table 4, the approximated natural angular frequencies belonging to the MDs are seen to be significantly higher than those of the mode shapes, cf. Table 3.

Table 4. Natural angular frequencies belonging to the MDs.

Frequency	Unit	Magnitude
ω_{11}	rad/s	50.99
ω_{21}	rad/s	38.58
ω_{22}	rad/s	71.15
ω_{31}	rad/s	24.06
ω_{32}	rad/s	18.17
ω_{33}	rad/s	56.04

Figure 5 plots the simulated response found by solving the projected EOMs in (10) using the Taylor basis in (15). For comparison the nonlinear response illustrated in Figure 2 is also included in Figure 5. In order to emphasize that the latter response is evaluated by solving the un-projected EOMs in (1), this is referred to as the *full nonlinear solution* in the following. The

Taylor-based solution is simulated using the CDM and with a time step a hundred times larger than the one used in the full nonlinear solution, i.e., $\Delta t = 56$ ms. The difference in time step magnitudes is discussed in more detail in the following section.

The two responses in Figure 5 are seen to be very close along the entire time interval considered. A noticeable difference in the response amplitude is visible within the first few seconds. The differences are caused by the response contribution from the higher frequency modes only included in the full nonlinear simulation. As time passes, the effect of lower frequency modes becomes dominant, and the amplitude difference between the simulated responses decreases. However, the Taylor basis is concluded to display a very high precision based on the results in Figure 5.

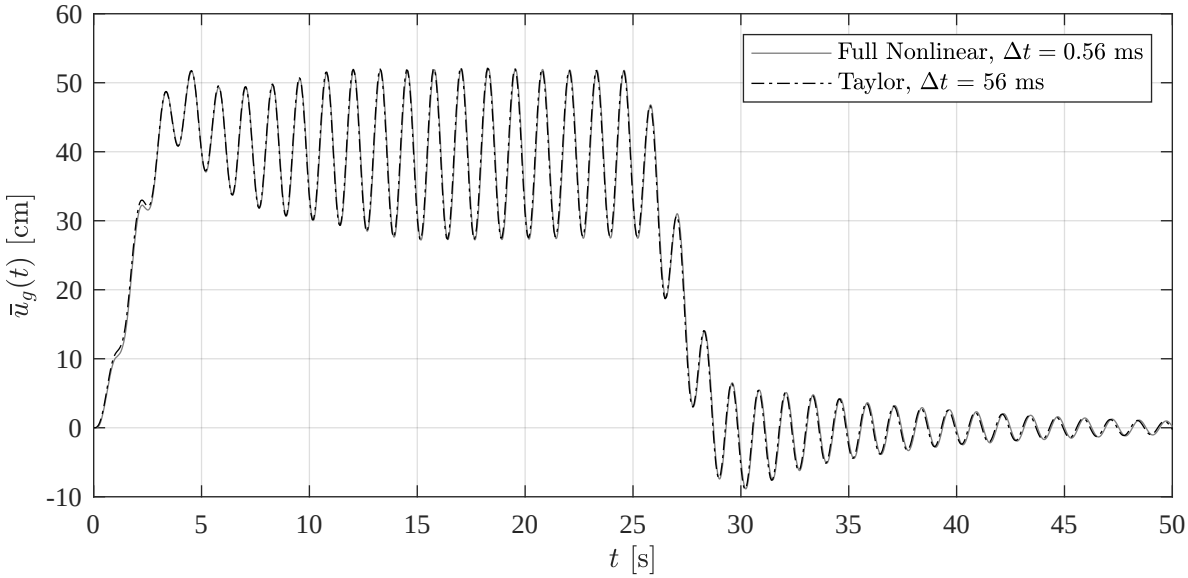

Figure 5. Kinematic nonlinear displacement $u_g(\ell/2, t)$ simulated by full nonlinear analysis and Taylor basis.

4.3. Time Integration Stability

The stability of the kinematic nonlinear simulations using a Taylor basis projection is analyzed. Specifically, the maximum allowed time step that ensures that the CDM time integration scheme remains stable is considered, referred to as the time step stability limit.

The analysis is performed considering the response of the damped bridge simulated using the Taylor basis in (15). The time step stability limit is considered within a linear to a highly nonlinear range by introducing a load scale $\beta \in [0.1, 3]$ multiplied simultaneously onto all loads in Table 2. The higher the value of β, the more significant the nonlinear effects are. Contrary, as $\beta \to 0$, the nonlinear effects will vanish. A value $\beta = 3$ is considered an extreme load case for the given structural system.

In Figure 6 two relative time steps limits, r_{i}, i ϵ [1,2] are plotted as a function of β. The ratio r_1 is defined (17) given as the Taylor basis time step stability limit, $\Delta t^{\mathrm{lim}}_{\mathrm{Taylor}}$, relative to the analytical time step stability limit for a linear CDM integration scheme, $\Delta t^{\mathrm{lim}}_{\mathrm{CDM}}$, including

only three mode shapes;

$$r_1 = \frac{\Delta t^{\text{lim}}_{\text{Taylor}}}{\Delta t^{\text{lim}}_{\text{CDM}}} \quad , \quad \Delta t^{\text{lim}}_{\text{CDM}} = \frac{2}{\omega_3} = 0.28 \text{ s} \tag{17}$$

where ω_3 refers to the value in Table 3. The ratio r_2 defines the Taylor basis time step stability limit relative to the time step stability limit of the full nonlinear analysis, $\Delta t^{\text{lim}}_{\text{Non}}$;

$$r_2 = \frac{\Delta t^{\text{lim}}_{\text{Taylor}}}{\Delta t^{\text{lim}}_{\text{Non}}} \quad , \quad \Delta t^{\text{lim}}_{\text{Non}} = 5.63 \cdot 10^{-4} \text{ s} \tag{18}$$

The value $\Delta t^{\text{lim}}_{\text{Non}}$ was found to be independent of the load scale β in the conducted analysis.

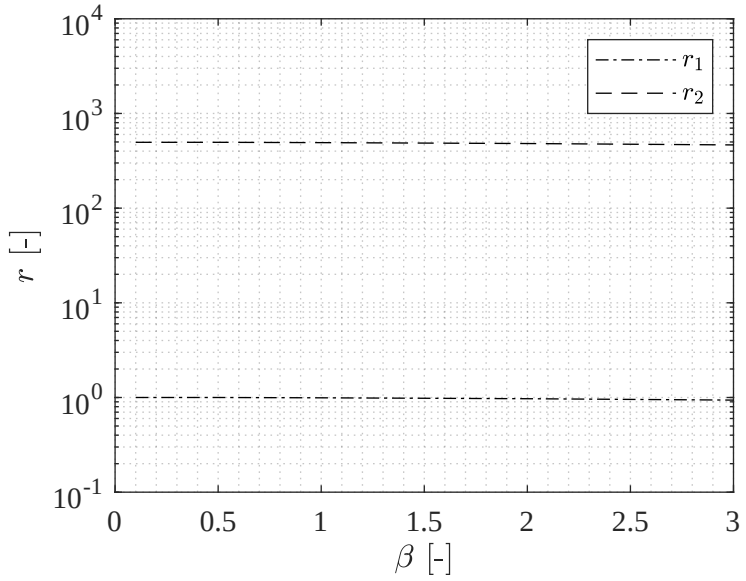

Figure 6. Relative time step stability limits, r, vs the load scale β.

From Figure 6, the ratio r_1 is seen to be very close to a value of one for the entire load scale interval considered. The ratio r_2 is significantly higher and is in the order of magnitude of four to five hundred within the considered interval. As the load scale β increases, minimal ratio decreases are observed.

Given that the ratio $r_1 \approx 1$, it can be concluded that the stability of the CDM time integration scheme when using Taylor basis projection for simulating kinematic nonlinear structures appears to be more or less identical to the time step stability limit derived for linear systems. Thus, the algorithm stability appears unaffected by the system nonlinearities, although high-frequency MDs are included in the basis.

In order to represent the response of a given mode shape to a reasonable degree in a simulation context, it is a good rule of thumb to use a time step, Δt, of a maximum one-tenth of its period length, T. Considering a Taylor basis simulation, it is primarily the response contributions from the mode shapes that are of interest to represent well. The MDs are also crucial for the overall solution, but their primary 'task' is to prevent an artificial stiffness increase, see e.g., [20]. Thus, for a Taylor basis including N mode shapes, a time step magnitude equal to one-tenth of the N'th mode shape period, T_N, is a reasonable choice.

$$\Delta t = \frac{1}{10}\text{T}_N = \frac{1}{10}\frac{2\pi}{\omega_N} = \frac{\pi}{10}\Delta t^{\text{lim}}_{\text{CDM}} = 0.31\Delta t^{\text{lim}}_{\text{CDM}} \tag{19}$$

As illustrated in (19), a time step equal to one-tenth of T_N is significantly smaller than the time step stability limit from linear analysis. Thus, following the rule of thumb concerning time step magnitudes, stability will likely not be an issue using Taylor basis projection.

5. Conclusion

The stability of the central difference time integration scheme using Taylor basis projection has been studied. The stability study was made by considering the response of a kinematic nonlinear beam bridge exposed to moving loads multiplied by a varying load scale. The analysis showed that the time step stability limit using Taylor basis projection was more or less identical to the analytical time step stability limit derived for linear systems. Furthermore, the time step stability limit using Taylor basis projection was two orders of magnitude higher than the time step stability limit solving the un-projected equations of motion. The superior stability properties using Taylor basis projecting made it possible to simulate the response of the kinematic nonlinear beam bridge with high accuracy using a time step one hundred times higher compared to solving the un-projected equations. Based on the described observations, it is concluded that Taylor basis projection displays superior stability properties that can significantly increase the time step magnitudes and, thereby, potentially significantly reduce the number of time steps and computational time.

References

[1] Horri K and Kawahara M 1969 *Proceedings of 19th Japan National Congress for Applied Mechanics* 17–22
[2] Nickell R E 1976 *Computer Methods in Applied Mechanics and Engineering* **7**(1) 107–129
[3] Lülf F A, Tran D M and Ohayon R 2013 *Journal of Sound and Vibration* **332**(15) 3897–3921
[4] Idelsohn S R and Cardona A 1984 Recent advances in reduction methods in nonlinear structural dynamics *Proceedings of the Second International Conference on: Recent Advances in Structural Dynamics* vol 2 (University of Southampton, England) pp 475–482
[5] Wilson E L, Yuan M W and Dickens J M 1982 *Earthquake Engineering & Structural Dynamics* **10**(6) 813–821
[6] Chaturantabut S and Sorensen D C 2010 *SIAM Journal on Scientific Computing* **32**(5) 2737–2764
[7] Carlberg K, Bou-Mosleh C and Farhat C 2011 *International Journal for Numerical Methods in Engineering* **86**(2) 155–181
[8] Amsallem D, Zahr M J and Farhat C 2012 *International Journal for Numerical Methods in Engineering* **92**(10) 891–916
[9] Idelsohn S R and Cardona A 1985 *Computer Methods in Applied Mechanics and Engineering* **49**(3) 253–279
[10] Idelsohn S R and Cardona A 1985 *Computers & Structures* **20**(1-3) 203–210
[11] Weeger O, Wever U and Simeon B 2014 *Computational Mechanics* **54**(6) 1477–1495
[12] Barbic J and James D 2005 *ACM Transactions on Graphics* **24**(3) 982–990
[13] Weeger O, Wever U and Simeon B 2016 *International Journals for Numerical Methods in Engineering* **108**(13) 1579–1602
[14] Slaats P M A, de Jongh J and Sauren A A H J 1995 *Computer & Structures* **54**(6) 1155–1171
[15] Andersson L, Persson P and Persson K 2023 *Mechanical Systems and Signal Processing* **191** 110143
[16] Brake M and Segalman D 2010 *The American Institute of Aeronautics and Astronautics* **48**(10) 2339–2347
[17] Tiso P, Jansen E and Abdalla M 2011 *Aiaa Journal* **49**(10) 2295–2304
[18] Andersen S and Poulsen P N *Earthquake Engineering & Structural Dynamics* **48** 989–1006
[19] Andersen S and Poulsen P N *Earthquake Engineering & Structural Dynamics* **48** 929–948
[20] Andersen S and Poulsen P 2014 Reduction method for real-time simulations in hybrid testing *Proceedings of EURODYN 2014* pp 1867–1874